

# The Application of Semisupervised Attentional Generative Adversarial Networks in Desert Seismic Data Denoising

Yue Li<sup>✉</sup>, Xinxing Luo<sup>✉</sup>, Ning Wu<sup>✉</sup>, and Xintong Dong<sup>✉</sup>

**Abstract**—For imaging and interpretation, high-quality seismic data are necessary. However, noise, which is strong in field desert seismic data, inevitably diminishes the quality of the data and reduces the signal-to-noise ratio. Moreover, the effective signals and noise in field desert seismic data are mostly distributed in the low-frequency band, which leads to severe spectral aliasing. Recently, some deep learning methods have improved the quality of desert seismic data in certain aspects. However, due to limitations of their networks and the serious spectral aliasing of desert seismic data, the denoising results usually show some false seismic reflections. To solve the above problems, we introduce Unsupervised Generative Attentional Networks with Adaptive Layer-Instance Normalization for Image-to-Image Translation (U-GAT-IT) to the denoising of desert seismic data in a semisupervised manner. U-GAT-IT is an unsupervised attentional generative adversarial network (GAN) combined with an attention module guided by the class activation map (CAM). The attention module guided by the CAM can guide the model to better distinguish between noise and effective signals. The experiment shows that the U-GAT-IT can effectively suppress desert seismic noise. Also, the denoising result has fewer false seismic reflections.

**Index Terms**—Class activation map (CAM), deep learning (DL), desert seismic data, generative adversarial networks (GANs).

## I. INTRODUCTION

SEISMIC exploration is an essential method for solid resource exploration, oil and gas exploration, and engineering geology research [1]–[3]. Seismic exploration enables the analysis of seismic data to infer the structure and lithology of the layer [4]. However, in field seismic exploration, seismic data are inevitably mixed with background noise [1], [2], [5], which leads to a low signal-to-noise ratio (SNR) and poor resolution of the data. Low-quality seismic data affect subsequent seismic analysis, such as imaging, inversion, and formation interpretation. For this reason, denoising is usually an indispensable part of seismic data processing.

Manuscript received December 15, 2020; revised February 22, 2021; accepted March 20, 2021. Date of publication April 28, 2021; date of current version December 31, 2021. This work was supported in part by the National Natural Science Foundation of China under Grant 41730422 and in part by the Cross Disciplinary Research Support Project for Doctoral Candidates of Jilin University under Grant 101832020DJX062. (*Corresponding author: Ning Wu*)

The authors are with the Department of Information, College of Communication Engineering, Jilin University, Changchun 130012, China (e-mail: liyue@jlu.edu.cn; 1783057427@qq.com; ning1337@gmail.com; 18186829038@163.com).

Digital Object Identifier 10.1109/LGRS.2021.3073419

Different from plains, hills, and other areas, desert areas are more open, which results in greater noise energy in desert seismic data. This severely reduces the SNR of the data [6]. Moreover, spectral aliasing is more severe [3], [5], [6]. Sand is the main medium of noise propagation in desert areas, and it can absorb most of the high-frequency noise [7]. Therefore, the frequency band of noise in desert seismic data is mostly concentrated at low frequencies. In addition, the effective signals are mostly concentrated in the low-frequency band. Therefore, separating effective signals and noise is indeed a daunting challenge.

At present, there are many classic methods for denoising seismic data, such as the wavelet transform [8], F-X deconvolution [9], and empirical mode decomposition [10]. Although these methods can improve the quality of seismic data in certain aspects, the aforementioned methods still have difficulty in reaching the standard for high-quality exploration. Recently, in terms of seismic data denoising, some deep learning (DL) methods have gradually emerged [11], [12]. Usually, these methods supervised learning to realize the mapping relationship between noisy data and clean data. However, due to the limitations of the networks and the serious spectral aliasing of desert seismic data, the denoising results usually show some false seismic reflections. Therefore, we try to find new DL methods to apply to desert seismic data denoising.

The generative adversarial networks (GANs) [13] are a type of DL network. The performance of GAN can be improved by the competition between the discriminator and the generator. The class activation map (CAM), proposed by Zhou *et al.* [14] in 2016, is a technology that can determine important parts by acquiring attention maps. Unsupervised Generative Attentional Networks with Adaptive Layer-Instance Normalization for Image-to-Image Translation (U-GAT-IT) [15] is a variant of the GAN. It has an attention module combined with the CAM. With the help of the attention map obtained by the CAM, the attention module can guide the model to distinguish between noise and effective signals and guide the mapping to concentrate on more important parts. Therefore, compared with previous DL networks, U-GAT-IT can obtain better denoising results.

We introduce U-GAT-IT to desert seismic data denoising in a semisupervised manner. In order to train U-GAT-IT, a training set containing a noisy seismic signal training set and a clean seismic signal training set is constructed. Moreover, the combination of adversarial loss, cycle loss, and CAM loss is taken as the total loss function. By training U-GAT-IT,

a denoising model that can map the noisy seismic data domain to the clean seismic data domain is obtained.

## II. METHOD

In this section, we will describe the construction of the training set, the basic architecture of U-GAT-IT, the loss function, and the denoising principle of U-GAT-IT in detail.

### A. Construction of the Training Set

We need to build clean and noisy seismic data training sets to meet the requirements of model training. However, it is difficult for us to obtain clean data from field seismic exploration. Therefore, Ricker wavelets, zero-phase wavelets, and mixed-phase wavelets were used to build a clean seismic data training set. Their specific equations are as follows:

$$f(t) = A[1 - 2 \times (\pi f_0(m - m_0))^2] \times e^{-(\pi f_0(m - m_0))^2} \quad (1)$$

$$f(t) = A \cos[2\pi f_0(m - m_0)] \times e^{-\left(\frac{2\pi f_0(m - m_0)}{r_1}\right)^2} \quad (2)$$

$$f(t) = A \sin[2\pi f_0(m - m_0)] \times e^{-\left(\frac{2\pi f_0(m - m_0)}{r_2}\right)^2} \quad (3)$$

where  $A$ ,  $f_0$ , and  $m_0$  are the amplitude, main frequency, and start time, respectively,  $m$  denotes the time, and  $r_1$  and  $r_2$  are used to adjust the waveforms. In this letter, the three wavelets mentioned above were used to simulate clean data. We generated 100 clean data with a size of  $1000 \times 200$  (number of sampling points  $\times$  number of traces) and turned these data into patches with dimensions of  $200 \times 200$ . Finally, we obtained a clean seismic data training set,  $T = \{t_1, t_2, \dots, t_g\}$ .

We used field noisy seismic data to construct a noisy seismic data training set. Field noisy seismic data can improve the performance of the trained model when processing field seismic data. In this letter, the field seismic data we used are from the Tarim region in China. The sampling interval, the number of traces, and the number of sampling points of these field seismic data are 2 ms, 200, and 5000, respectively. Then, we used a  $200 \times 200$  sliding window to intercept some patches with obvious seismic signals. Finally, we obtained a noisy seismic data training set,  $S = \{s_1, s_2, \dots, s_e\}$ .

### B. Basic Architecture of U-GAT-IT

The framework of U-GAT-IT includes two generators, named  $G_{s \rightarrow t}$  and  $G_{t \rightarrow s}$ , and two discriminators, named  $D_s$  and  $D_t$ . U-GAT-IT integrates the attention module combined with the CAM into the generator and discriminator. The main idea of the CAM is to extract the feature maps by convolutional neural networks and obtain the weights corresponding to these maps by global average pooling. Then, the feature maps are multiplied by the weights and added directly to obtain the attention feature map. The generation of the attention feature map is shown in Fig. 1. This map plays a role in guiding and improving network training. The attention module guide in the discriminator focuses on the parts that are essential for generating the denoising signal. The attention module in the generator focuses on the difference between effective signals and noise. The input of U-GAT-IT is clean data  $S$  and noisy data  $T$ , which are used to realize the mutual conversion

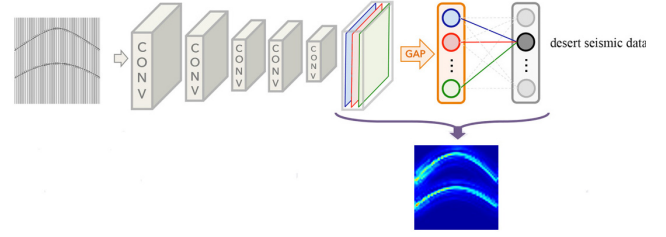


Fig. 1. Generation of the attention feature map.

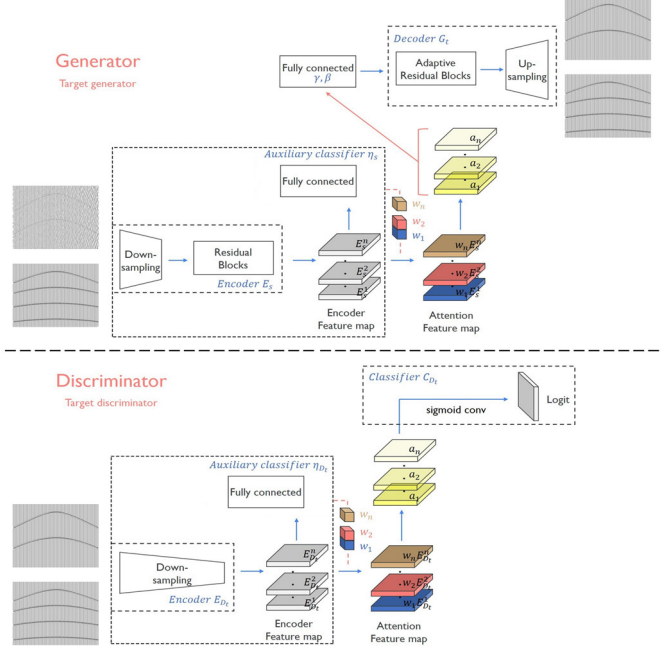


Fig. 2. Basic architecture of U-GAT-IT.

between clean data and noisy data. For ease of understanding, we only introduce the conversion of noisy data into clean data, as shown in Fig. 2.

The generator  $G_{s \rightarrow t}$  is composed of an encoder  $E_s$ , an auxiliary classifier  $\eta_s$ , and a decoder  $G_t$ . Let  $x \in \{X_s, X_t\}$  denote the noisy and clean data. The input noisy data pass through the downsampling module and residual blocks in the encoder to obtain the encoded feature map  $\{E_s^1(x), E_s^2(x), \dots, E_s^n(x)\}$ , where  $n$  represents the number of feature maps. The encoded feature map is divided into two paths. One path passes through the auxiliary classifier used to obtain the weight information  $w$  of the feature maps and is then multiplied by the other encoded feature map to obtain the attention feature map. The attention feature map passes through a  $1 \times 1$  convolutional layer, where the activation function is the rectified linear unit, and the feature map  $\{a_1, a_2, \dots, a_n\}$  is obtained. Then, the feature map is used as the input of the decoder. The generated result maintaining the detailed dynamic characteristics is obtained with the help of an adaptive residual block and an upsampling module. The adaptive residual block combines Adaptive Layer-Instance Normalization (AdaLIN), and AdaLIN can be expressed as follows:

$$\hat{a}_I = \frac{a - \mu_I}{\sqrt{\sigma_I^2 + \epsilon}}, \quad \hat{a}_L = \frac{a - \mu_L}{\sqrt{\sigma_L^2 + \epsilon}} \quad (4)$$

$$\begin{aligned} \text{AdaLIN}(a, \gamma, \beta) &= \gamma \cdot (\rho \cdot \hat{a}_L + (1 - \rho) \cdot \hat{a}_L) + \beta \quad (5) \\ \rho &\leftarrow \text{clip}_{[0,1]}(\rho - \tau \Delta\rho) \end{aligned}$$

where  $\mu_I$  and  $\mu_L$  and  $\sigma_I$  and  $\sigma_L$  are the means and standard deviations of the channel and layer, respectively,  $\gamma$  and  $\beta$  represent the parameters generated by the connected layer,  $\tau$  denotes the learning rate,  $\rho$ , the value of which is limited to the range of [0,1], denotes the value related to AdaLIN, and  $\Delta\rho$  represents the parameter update vector determined by the optimizer. AdaLIN helps to solve the conversion problem between domains by selectively retaining or changing content information.

The discriminator  $D_t$  is composed of an encoder  $E_{D_t}$ , a classifier  $C_{D_t}$ , and an auxiliary classifier  $\eta_{D_t}$ . The structure of the discriminator is similar to that of the generator, but there are no residual blocks in the encoder. The activation function of the classifier is the sigmoid function. The main function of the discriminator is to output the probability of the result of the classifier to the generator so that the generator can output more accurate results.

### C. Loss Function

We mainly use the loss function to optimize the performance of the model. In order to enable U-GAT-IT to achieve the functions we need, we take the combination of the adversarial loss, cycle loss, and CAM loss as the total loss function. These three losses can be expressed as

$$L_{\text{gan}}^{s \rightarrow t} = E_{x \sim X_t} [(D(x))^2] + E_{x \sim X_s} [(1 - D_t(G_{s \rightarrow t}(x)))^2] \quad (7)$$

$$L_{\text{cycle}}^{s \rightarrow t} = E_{x \sim X_s} [|x - G_{t \rightarrow s}(G_{s \rightarrow t}(x))|_1] \quad (8)$$

$$L_{\text{cam}}^{s \rightarrow t} = -(E_{x \sim X_s} [\log(\eta_s(x))] + E_{x \sim X_t} [\log(1 - \eta_s(x))]) \quad (9)$$

$$L_{\text{cam}}^{D_t} = E_{x \sim X_t} [(\eta_{D_t}(x))^2] + E_{x \sim X_s} [(1 - \eta_{D_t}(G_{s \rightarrow t}(x)))^2] \quad (10)$$

where  $\eta_s(x)$  and  $\eta_{D_t}(x)$  represent the encoded feature map sent to the auxiliary classifier in the generator and the encoded feature map sent to the auxiliary classifier through the discriminator, respectively.

The adversarial loss matches the distribution of the denoised data with the distribution of the clean data. The cycle loss ensures that a cycle consistency constraint is applied to the generator and mitigates the pattern collapse problem. The CAM loss improves the performance of the model by using the information in auxiliary classifiers  $\eta_s$  and  $\eta_{D_t}$ .

Finally, the encoder, decoder, discriminator, and auxiliary classifier are jointly trained to optimize the final goal

$$\min_{G_{s \rightarrow t}, G_{t \rightarrow s}, \eta_s, \eta_{D_t}} \max_{D_s, D_t, \eta_{D_s}, \eta_{D_t}} \lambda_1 L_{\text{gan}} + \lambda_2 L_{\text{cycle}} + \lambda_3 L_{\text{cam}} \quad (11)$$

where  $\lambda_1 = 1$ ,  $\lambda_2 = 10$ , and  $\lambda_3 = 1000$ . Here,  $L_{\text{gan}}$  is the sum of  $L_{\text{gan}}^{s \rightarrow t}$  and  $L_{\text{gan}}^{t \rightarrow s}$ . The definitions of  $L_{\text{cycle}}$  and  $L_{\text{cam}}$  are similar.

### D. Denoising Principle of U-GAT-IT

The field desert seismic data can be described as

$$s = t + n \quad (12)$$

where  $s$ ,  $t$ , and  $n$  represent noisy data, clean data, and desert noise, respectively. To convert the noisy data  $s$  back to clean data  $t$ , we need to obtain a denoising model that can map the noisy seismic data domain to the clean seismic data domain. We use the Adam algorithm to optimize U-GAT-IT, and the learning rate and the number of iterations are fixed at  $1e^{-4}$  and 500, respectively. The denoising model  $G$  generated by training is used to realize the mapping from  $s$  to  $t$ . Denoising can be described as the mapping of noisy data  $s$  to the predicted clean data  $\hat{t}$

$$\hat{t} = G(s). \quad (13)$$

### III. PROCESSING OF SYNTHETIC DATA

In this section, we process and analyze synthetic seismic data. We use the PyTorch framework to train and test U-GAT-IT, and the clean training set is generated in MATLAB. The model training takes 10 h and 54 min in total. Then, we use the generator network of  $G$  (we call it the U-GAT-IT denoiser) to denoise the synthetic seismic data. Moreover, we compare the U-GAT-IT denoiser with the wavelet transform, F-X deconvolution, and denoising convolutional neural network (DnCNN) to analyze the performance of the denoiser.

We construct four sets of synthetic seismic data, including synthetic clean seismic data, low-frequency synthetic desert seismic random noise, and synthetic noisy seismic data with different SNRs, to test the U-GAT-IT denoiser. To evaluate the denoising performance of the U-GAT-IT denoiser, we separately analyze the denoising results, the predicted noise, and their F-K spectrum. Moreover, we use the SNR and mean squared error (MSE) to represent the denoising performance of the wavelet transform, F-X deconvolution, DnCNN denoiser, and U-GAT-IT denoiser. The formulas of the SNR and MSE are as follows:

$$\text{SNR} = 10 \log_{10} \left( \frac{\sum_{i=1}^N \sum_{j=1}^M (T(i, j) - \bar{T})^2}{\sum_{i=1}^N \sum_{j=1}^M (\hat{S}(i, j) - T(i, j))^2} \right) \quad (14)$$

$$\text{MSE} = \frac{1}{N \times M} \sum_{i=1}^N \sum_{j=1}^M (\hat{S}(i, j) - T(i, j))^2 \quad (15)$$

where  $T$  represents the clean signal,  $\bar{T}$  represents the average value of  $T$ ,  $\hat{S}$  denotes the processed record, and  $M$  and  $N$  represent the trace and the number of samples, respectively. A better denoising effect usually has a larger SNR and a smaller MSE.

In Fig. 3, we show a set of synthetic seismic data and their F-K spectrum. The number of traces of the synthetic clean seismic data, the number of sampling points of each trace, and the spatial and temporal sampling intervals are 200, 1000, 5 m, and 2 ms, respectively. The synthetic clean seismic data in Fig. 3(a) are superimposed with the low-frequency synthetic desert seismic random noise in Fig. 3(b) to obtain the synthetic noisy seismic data in Fig. 3(c).

To compare the effects of these four methods, we show the denoising results of these methods in Fig. 4. By comparison, Fig. 4 shows that more or less noise remains in Fig. 4(a)–(c), while there is basically no noise in Fig. 4(d). Moreover,

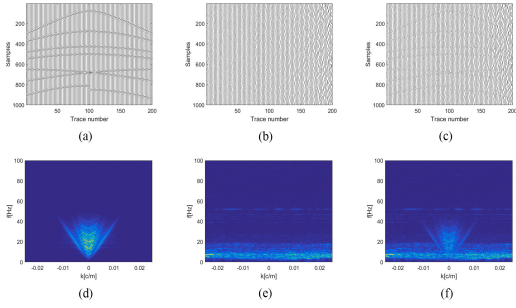


Fig. 3. Synthetic seismic data. (a)–(c) Synthetic clean seismic data, low-frequency synthetic desert seismic random noise, and synthetic noisy seismic data ( $\text{SNR} = -8.26 \text{ dB}$  and  $\text{MSE} = 0.3503$ ), respectively. (d)–(f) F-K spectrum of (a)–(c), respectively.

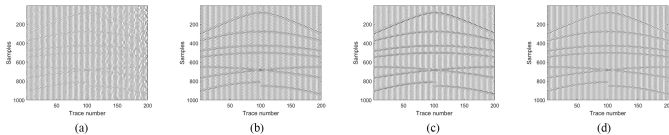


Fig. 4. Denoising results of four denoising methods. (a)–(d) Wavelet transform, F-X deconvolution, DnCNN denoiser, and U-GAT-IT denoiser, respectively.

TABLE I  
DENOISING RESULTS OF DIFFERENT METHODS [SNR/MSE]

Noisy data	Wavelet transform	F-X deconvolution	DnCNN denoiser	U-GAT-IT denoiser
$0.79/4.4 \times 10^{-2}$	$6.85/1.1 \times 10^{-2}$	$6.44/1.2 \times 10^{-2}$	$15.82/1.4 \times 10^{-3}$	$17.79/9.0 \times 10^{-4}$
$-2.54/9.4 \times 10^{-2}$	$4.09/2.1 \times 10^{-2}$	$5.36/1.5 \times 10^{-2}$	$15.09/1.6 \times 10^{-3}$	$17.22/1.0 \times 10^{-3}$
$-5.23/1.7 \times 10^{-1}$	$1.53/3.7 \times 10^{-2}$	$4.03/2.1 \times 10^{-2}$	$14.02/2.1 \times 10^{-3}$	$16.68/1.1 \times 10^{-3}$
$-8.26/3.5 \times 10^{-1}$	$-1.79/7.9 \times 10^{-2}$	$2.07/3.3 \times 10^{-2}$	$12.37/3.0 \times 10^{-3}$	$15.65/1.4 \times 10^{-3}$

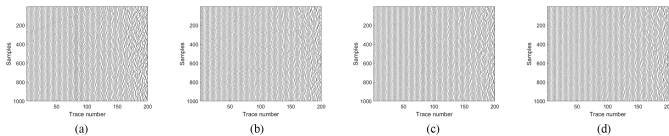


Fig. 5. Comparison of the predicted noise. (a)–(d) Wavelet transform, F-X deconvolution, DnCNN denoiser, and U-GAT-IT denoiser, respectively.

we show the denoising performance of these four methods on noisy data with different SNRs in Table I. Under the same conditions, the denoising result of the U-GAT-IT denoiser has a higher SNR and a smaller MSE, which means better denoising performance.

Then, we list the predicted noise of these methods in Fig. 5. By comparing the predicted noise in Fig. 5 with the noise in Fig. 3(b), we can conclude that the predicted noise of the U-GAT-IT denoiser, as shown in Fig. 5(d), is the most similar. Moreover, some effective signals are left in Fig. 5(a)–(c). This means that the U-GAT-IT denoiser has more advantages in processing synthetic noisy seismic data.

Finally, in order to make our conclusions more convincing, we obtain the F-K spectrogram of the denoising result and the predicted noise. They are shown in Figs. 6 and 7. In Fig. 6, we find that the corresponding results of the U-GAT-IT denoiser, as shown in Fig. 6(d), are the most similar to

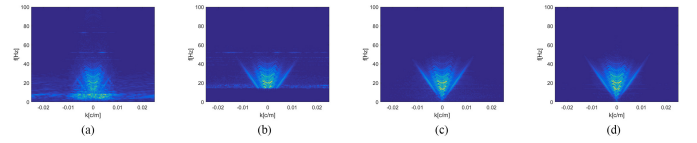


Fig. 6. Comparison of the F-K spectrum of denoising results. (a)–(d) F-K spectrum of the denoising results in Fig. 4.

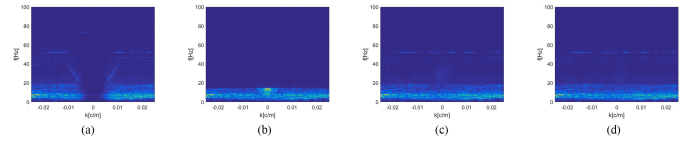


Fig. 7. Comparison of the F-K spectrum of predicted noise. (a)–(d) F-K spectrum of the predicted noise in Fig. 5.

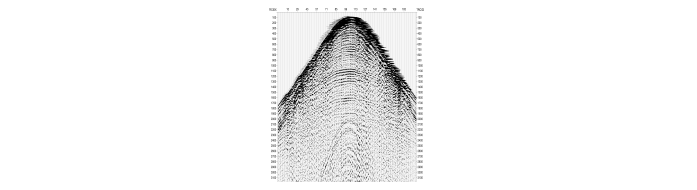


Fig. 8. Field common-shot-point record in the desert area.

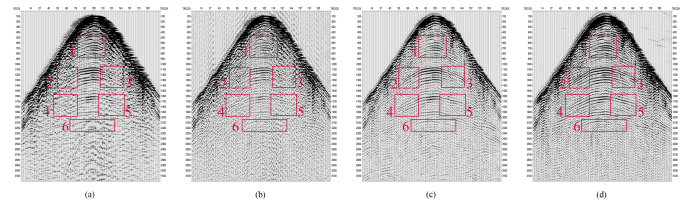


Fig. 9. Denoising results of the record in Fig. 8. (a)–(d) Denoising results of the record in Fig. 8 by using the wavelet transform, F-X deconvolution, DnCNN denoiser, and U-GAT-IT denoiser, respectively.

Fig. 3(d). Furthermore, in Fig. 7, we find that the corresponding result of the U-GAT-IT denoiser, as shown in Fig. 7(d), is the most similar to Fig. 3(e). These results further illustrate that the U-GAT-IT denoiser has more advantages in processing synthetic noisy seismic data.

#### IV. FIELD DATA PROCESSING

In this section, we compare the denoising results of the wavelet transform, F-X deconvolution, the DnCNN denoiser, and the U-GAT-IT denoiser on the field common-shot-point record in the desert area shown in Fig. 8. We obtain the data from the Tarim region in China. In these field data, there is considerable noise, including low-frequency noise and surface waves. The effective signals are affected by the noise and have poor continuity.

In the denoising results of the wavelet transform and F-X deconvolution, as shown in Fig. 9(a) and (b), part of the low-frequency noise and surface waves are suppressed. However, after processing, some low-frequency noise and surface waves remain in the results. In addition, the continuity of the effective signals in these rectangles is very poor. In the denoising results of the DnCNN denoiser, as shown in Fig. 9(c), although most of the low-frequency noise and surface waves

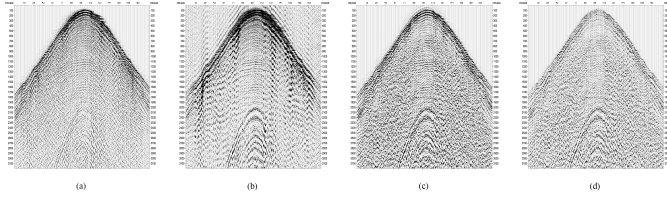


Fig. 10. Separated noise of the record in Fig. 8. (a)–(d) Separated noise of the record in Fig. 8 by using the wavelet transform, F-X deconvolution, DnCNN denoiser, and U-GAT-IT denoiser, respectively.

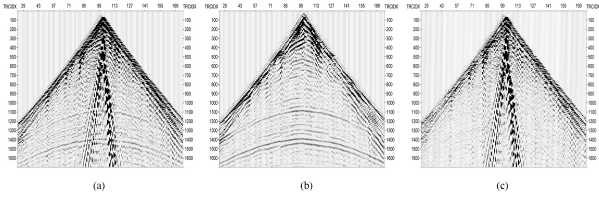


Fig. 11. Denoising results from another desert project. (a)–(c) Field common-shot-point record from different desert projects, the denoising result of U-GAT-IT denoiser, and the separated noise, respectively.

are suppressed, the continuity of the effective signals in these rectangles is not particularly good. In addition, there are some false seismic reflections in the bottom area of the DnCNN denoising results. In the denoising results of the U-GAT-IT denoiser, as shown in Fig. 9(d), most of the low-frequency noise and surface waves are suppressed. In these rectangles, the continuity of the effective signals is better, especially in rectangle 5. In addition, there are fewer false seismic reflections compared to the result of the DnCNN denoiser. As shown in Fig. 10, compared with the separated noise of the other three methods, there are fewer effective signals in the separated noise of the U-GAT-IT denoiser. Therefore, among the four methods, the amplitude preservation of the U-GAT-IT denoiser is the best. In general, compared with the other three methods, the U-GAT-IT denoiser has a better performance in suppressing low-frequency noise and surface waves and restoring the continuity of effective signals. In order to verify the generalization ability, we show the denoising results from another desert project. As shown in Fig. 11, although most of the low-frequency noise and surface waves are suppressed in the denoising results of the U-GAT-IT denoiser, there are a few very weak effective signals in the separated noise of the U-GAT-IT denoiser. Therefore, the U-GAT-IT denoiser has good generalization ability.

## V. CONCLUSION

Desert seismic data have serious spectral aliasing and are affected by low-frequency noise. These unique characteristics of desert seismic data make most denoising methods unable to denoise desert seismic data effectively. Recently, the application of DL in the denoising of desert seismic

data has effectively suppressed most of the noise. However, due to the limitations of the networks, the denoising results usually show some false seismic reflections. In this letter, to solve the aforementioned problems, we introduce U-GAT-IT to the denoising of desert seismic data and verify its superior performance by the corresponding experiments. The results of the experiments show that U-GAT-IT can effectively suppress the noise in desert seismic data, and the continuity of the effective desert seismic signals in the denoising results is also better. In addition, there are fewer false seismic reflections in the denoising result than in the result of the DnCNN denoiser, and the U-GAT-IT denoiser has good generalization ability.

## REFERENCES

- [1] N. Wu, Y. Li, and B. Yang, "Applications of the trace transform in surface wave attenuation on seismic records," *IEEE Trans. Geosci. Remote Sens.*, vol. 49, no. 12, pp. 4997–5007, Dec. 2011.
- [2] X. Dong *et al.*, "Signal-to-noise ratio enhancement for 3C down-hole microseismic data based on the 3D shearlet transform and improved back-propagation neural networks," *Geophysics*, vol. 84, no. 4, pp. V245–V254, Jul. 2019.
- [3] X. Dong, Y. Li, N. Wu, Y. Tian, and P. Yu, "The S-STK/LTK algorithm for arrival time picking of microseismic signals," *J. Geophys. Eng.*, vol. 15, no. 4, pp. 1484–1491, Aug. 2018.
- [4] E. C. David, N. Brantut, L. N. Hansen, and I. Jackson, "Low-frequency measurements of seismic moduli and attenuation in antigorite serpentinite," *Geophys. Res. Lett.*, vol. 46, no. 4, pp. 1993–2002, Feb. 2019.
- [5] H. Ma, J. Yan, Y. Li, C. Zhang, and H. Lin, "Desert seismic random noise reduction based on LDA effective signal detection," *Acta Geophys.*, vol. 67, no. 1, pp. 109–121, Feb. 2019.
- [6] G. Li, Y. Li, and B. Yang, "Seismic exploration random noise on land: Modeling and application to noise suppression," *IEEE Trans. Geosci. Remote Sens.*, vol. 55, no. 8, pp. 4668–4681, Aug. 2017.
- [7] T. Zhong, S. Zhang, Y. Li, and B. Yang, "Simulation of seismic-prospecting random noise in the desert by a Brownian-motion-based parametric modeling algorithm," *Comp. Rendus Geosci.*, vol. 351, no. 1, pp. 10–16, Jan. 2019.
- [8] S. M. Mousavi, C. A. Langston, and S. P. Horton, "Automatic microseismic denoising and onset detection using the synchrosqueezed continuous wavelet transform," *Geophysics*, vol. 81, no. 4, pp. V341–V355, Jul. 2016.
- [9] P. E. Harris and R. E. White, "Improving the performance of  $f-x$  prediction filtering at low signal-to-noise ratios," *Geophys. Prospecting*, vol. 45, no. 2, pp. 269–302, Mar. 1997.
- [10] J. L. Gómez and D. R. Velis, "A simple method inspired by empirical mode decomposition for denoising seismic data," *Geophysics*, vol. 81, no. 6, pp. V403–V413, Nov. 2016.
- [11] X. T. Dong, Y. Li, and B. J. Yang, "Desert low-frequency noise suppression by using adaptive DnCNNs based on the determination of high-order statistic," *Geophys. J. Int.*, vol. 219, no. 2, pp. 1281–1299, Nov. 2019.
- [12] W. Zhu, S. M. Mousavi, and G. C. Beroza, "Seismic signal denoising and decomposition using deep neural networks," *IEEE Trans. Geosci. Remote Sens.*, vol. 57, no. 11, pp. 9476–9488, Nov. 2019.
- [13] I. J. Goodfellow *et al.*, "Generative adversarial nets," in *Proc. Adv. Neural Inf. Process. Syst.*, 2014, pp. 2672–2680.
- [14] B. Zhou, A. Khosla, A. Lapedriza, A. Oliva, and A. Torralba, "Learning deep features for discriminative localization," in *Proc. IEEE Conf. Comput. Vis. Pattern Recognit. (CVPR)*, Jun. 2016, pp. 2921–2929, doi: 10.1109/CVPR.2016.319.
- [15] J. Kim, M. Kim, H. Kang, and K. Lee, "U-GAT-IT: Unsupervised generative attentional networks with adaptive layer-instance normalization for image-to-image translation," 2019, *arXiv:1907.10830*. [Online]. Available: <http://arxiv.org/abs/1907.10830>